



Near-Infrared Fluorescence Imaging for Noninvasive Trafficking of Scaffold Degradation

SUBJECT AREAS:
TISSUE ENGINEERING
FLUORESCENCE IMAGING
OPTICAL IMAGING
NANOSTRUCTURES

Soon Hee Kim^{1,2}, Jeong Heon Lee¹, Hoon Hyun¹, Yoshitomo Ashitate¹, GwangLi Park¹, Kyle Robichaud¹, Elaine Lunsford¹, Sang Jin Lee³, Gilson Khang² & Hak Soo Choi¹

¹Division of Hematology/Oncology, Department of Medicine, Beth Israel Deaconess Medical Center, Harvard Medical School, Boston, MA 02215, ²WCU Department of BIN Fusion Technology, Chonbuk National University, Jeonju 561-756, South Korea, ³Wake Forest Institute for Regenerative Medicine, Winston-Salem, NC 27101.

Received
29 November 2012

Accepted
18 January 2013

Published
5 February 2013

Correspondence and requests for materials should be addressed to S.J.L. (sjlee@wakehealth.edu) or G.K. (gskhang@jbnu.ac.kr) or H.S.C. (hchoi@bidmc.harvard.edu)

Biodegradable scaffolds could revolutionize tissue engineering and regenerative medicine; however, *in vivo* matrix degradation and tissue ingrowth processes are not fully understood. Currently a large number of samples and animals are required to track biodegradation of implanted scaffolds, and such nonconsecutive single-time-point information from various batches result in inaccurate conclusions. To overcome this limitation, we developed functional biodegradable scaffolds by employing invisible near-infrared fluorescence and followed their degradation behaviors *in vitro* and *in vivo*. Using optical fluorescence imaging, the degradation could be quantified in real-time, while tissue ingrowth was tracked by measuring vascularization using magnetic resonance imaging in the same animal over a month. Moreover, we optimized the *in vitro* process of enzyme-based biodegradation to predict implanted scaffold behaviors *in vivo*, which was closely related to the site of inoculation. This combined multimodal imaging will benefit tissue engineers by saving time, reducing animal numbers, and offering more accurate conclusions.

Tissue engineering offers attractive approaches for the reconstruction of damaged tissues and organs. The basic approach includes creating a neo-tissue by combining cells with biodegradable natural and/or synthetic polymeric scaffolds under suitable culture conditions, resulting in a tissue construct that can be implanted *in vivo* for bone, cartilage, musculoskeletal, and cardiovascular regeneration^{1–3}. The implanted scaffolds are eventually degraded and replaced by vascularized tissues over time, and the rate of scaffold degradation and tissue formation inside the scaffold must be equivalent for successful outcomes^{4,5}. Many efforts have focused on monitoring scaffold degradation behaviors by measuring changes in mechanical properties^{6,7}, and molecular weight^{6,8}, matrix weight⁹, morphology⁶, viscosity¹⁰; however, most of these methods require sacrifice of numerous animals at various time points, which often leads to inaccurate conclusions, as there can be broad batch-to-batch and animal-to-animal variations.

To avoid these pitfalls, longitudinal monitoring of scaffold degradation and cell/tissue ingrowth using non-invasive imaging modalities has been attempted. The feasibility of using ultrasound elasticity imaging was demonstrated to measure mechanical properties and degradation of implanted scaffolds¹¹, while magnetic resonance imaging (MRI) has been applied to track implanted cells pre-labeled with ferumoxides¹². Real-time optical fluorescence imaging techniques have also been applied for *in situ* monitoring of implanted biomaterials^{13,14}. Most recently, Artzi et al. demonstrated noninvasive assessment of implanted hydrogels sequentially to model hydrolytical and enzymatical degradation of biomaterials¹⁵. However, the result from *in vitro* was still far from accurate to predict *in vivo* biodegradation behaviors because of the physical, chemical, and optical instability of the visible wavelength fluorophore used for the study. Also, endogenous tissue autofluorescence in the visible wavelength range limits the use of such conventional fluorophores *in vivo*¹⁶.

To overcome these limitations, we engineered biodegradable scaffolds using an invisible near-infrared (NIR) fluorophore having excellent optical properties and high physicochemical stability in serum and in the body, which enabled longitudinal monitoring of scaffold degradation *in vivo*. Moreover, the NIR fluorescence imaging (700–900 nm) eliminates autofluorescence from the body, which can increase accuracy of imaging data from animals^{17–19}. In addition, we applied noninvasive and nonirradiant MRI to assess tissue ingrowth by observing vascularization during neo-tissue formation.



Results

Engineering biodegradable NIR scaffolds. The extracellular matrix (ECM) scaffold derived from porcine small intestinal submucosa (SIS) has been extensively characterized and used in the various fields of tissue engineering^{20–23}. As shown in Fig. 1a, the NIR fluorescent biodegradable scaffold was prepared by conjugating ZW800-1 *N*-hydroxysuccinimide (NHS) ester to the collagen unit on the crosslinked SIS scaffold. The zwitterionic NIR fluorophore ZW800-1 presents stable physicochemical and optical properties in collagenase buffers (Fig. 1b) as well as no measurable toxicity in mice, rats, and pigs^{17,19,24}. The physical integrity of the scaffold such as surface and cross-sectional gross morphology was preserved after NIR fluorophore conjugation (Fig. S1). To engineer a highly bright scaffold, various labeling ratios were demonstrated, and the contrast-to-background ratio (CBR) was calculated by measuring NIR fluorescence signals (see **Online Methods** and Fig. S2). The highest CBR without quenching was observed when the ratio of dye against the collagen unit was around 1 (labeling ratio ≈ 0.5), and we used this labeling ratio to prepare NIR scaffolds for the rest of study (Table S1).

Quantitation of scaffold degradation *in vitro*. To quantify the degree of scaffold degradation *in vitro*, we measured signal reduction in the NIR scaffolds using the FLARETM imaging system over a month. Since interstitial collagenase breaks down type I collagen that is abundant in SIS scaffold ($>90\%$ protein)²⁰, we prepared various concentrated collagenase buffers (0–1 mg/mL) to find the best condition to predict *in vivo* scaffold degradation. The rate of scaffold degradation was monitored by measuring changes in NIR fluorescence signals from the scaffold. The scaffold degradation facilitated proportionally to the collagenase concentration (Fig. S3a), and the NIR fluorescence signal decreased over the incubation time (Fig. 2a). Indeed, almost no NIR signal was found from the scaffold at D28 incubation in 1 mg/mL collagenase buffer. However, the shape of scaffold was not changed significantly because the collagen-based scaffold shows enzyme-mediated bulk erosion, and the degraded NIR-conjugated collagen units are diffused out from the scaffold²⁵. To confirm the biodegradation rate of NIR scaffolds, we collected incubation solutions at each time point and quantitated the released amount of dyes (Fig. S3b). The NIR scaffold incubated in phosphate buffer without collagenase was used as a control to compensate the

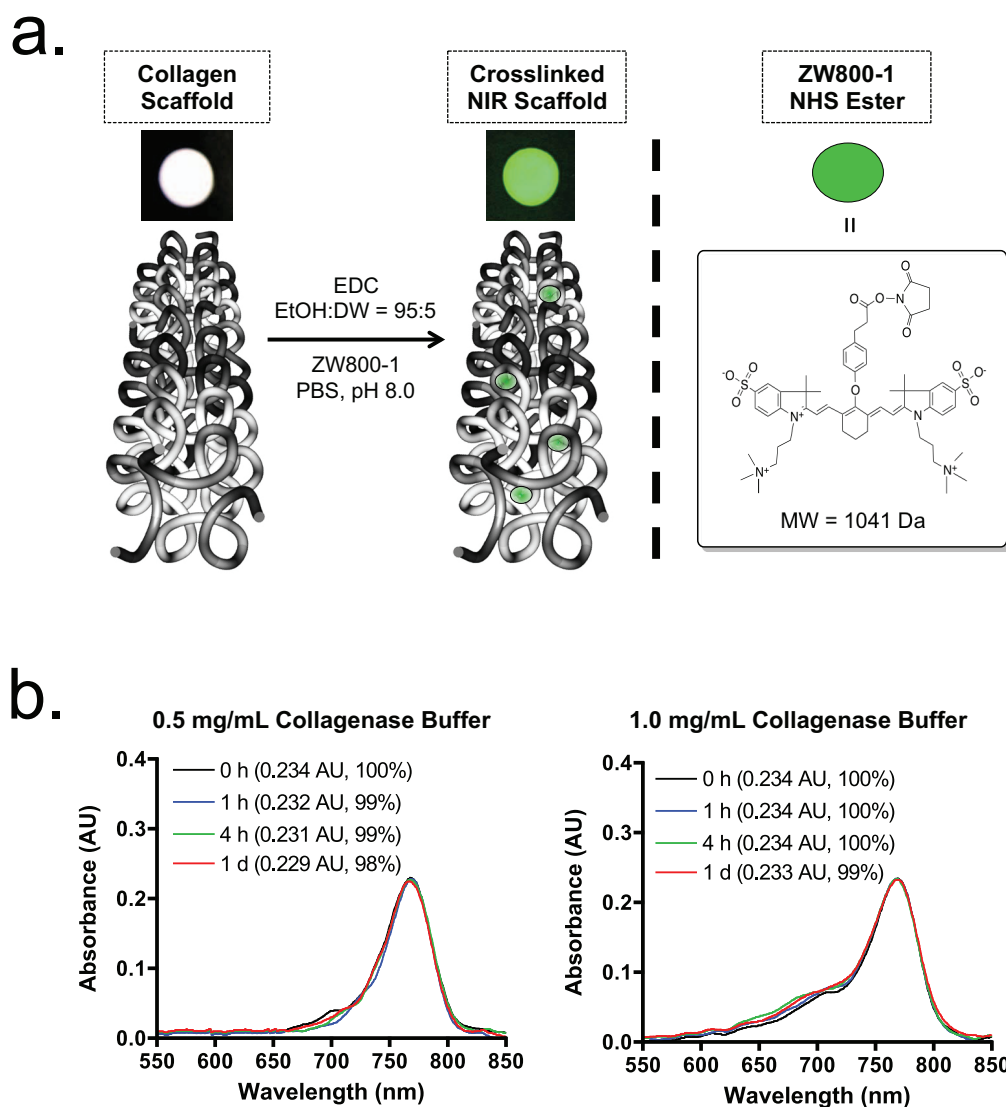


Figure 1 | Preparation of NIR fluorophore-conjugated collagen scaffold. (a) Schematic drawing of NIR scaffold preparation and chemical structure of ZW800-1 NHS ester. (b) Optical property and stability of ZW800-1 (10 μM) in collagenase buffer. Shown are absorbance spectra measured after 10-fold dilution in working buffer (extinction coefficient = 234,000 $\text{L mol}^{-1} \text{cm}^{-1}$ in collagenase buffer).

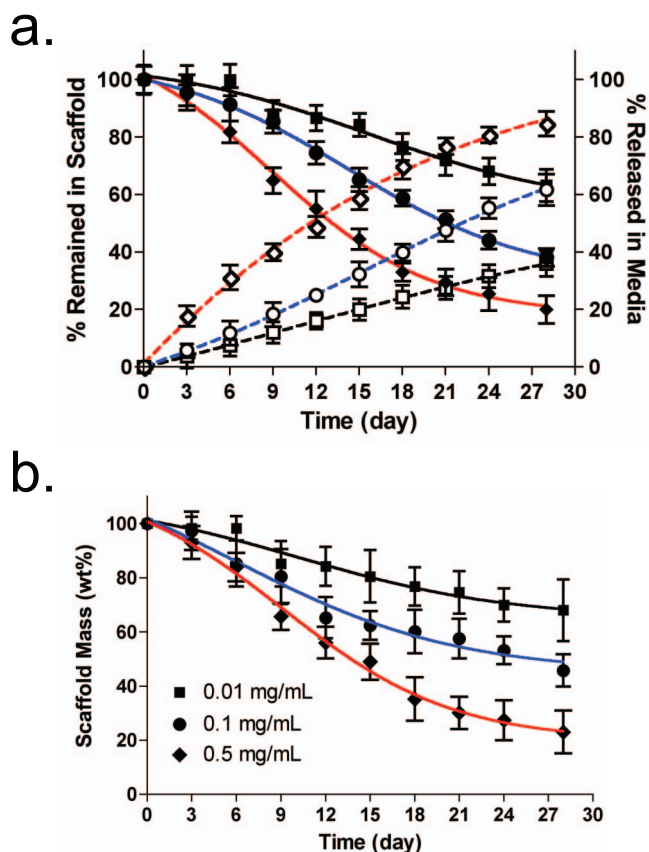


Figure 2 | Quantification of *in vitro* scaffold degradation in collagenase buffers. (a) Optical measurement of NIR fluorophores in scaffolds (black symbols, solid lines) and in the released solutions (white symbols, dotted lines). (b) Conventional scaffold degradation profiles by measuring weight loss. ■, □ = 0.01 mg/mL; ●, ○ = 0.1 mg/mL; ◆, ◇ = 0.5 mg/mL collagenase. The weight was measured after drying scaffolds completely for 2 days. Each data point is the mean \pm S.D. from N = 5 scaffolds.

signal loss from intact fluorophore in scaffolds and solutions. In the early phase, relatively high signals were found in buffer solutions because of rapid degradation of non-crosslinked collagen units, which were diffused out from the collagen matrix. As summarized in Fig. 2a, gradual signal reduction was observed in the scaffold over 28 days, while proportional signal increase was measured in the accumulated incubation buffer. Therefore, signal reduction in the scaffold reflects degradation of NIR-conjugated collagen units from the scaffold.

As a gold standard for scaffold degradation measurement, we performed a gravimetric assay that has been commonly used in the field of tissue engineering to provide the absolute value of mass changes in the scaffold. At least 5 samples were taken at each time incubation point and lyophilized to measure the remaining mass. As shown in Fig. 2b, the scaffolds in various collagenase buffers showed a very similar degradation pattern with the result from optical fluorescence measurement. Using fluorescence microscopy, we confirmed that the cross-section of the NIR scaffold collapsed gradually over collagenase concentrations with significant reduction in fluorescence signals (Fig. S4). This result indicates that the fluorescence signal reduction corresponds to the proportional biodegradation of NIR scaffolds.

Quantitation of scaffold degradation *in vivo*. To investigate the effect of local enzyme amount-mediated biodegradation in the body, NIR scaffolds were implanted into the subcutaneous pocket of axilla and thigh region separately. It is known that mechanical stress

around the implanted scaffold is a major determining factor for the degree of the foreign body reaction²⁶, which stimulates collagenase production and release from fibroblasts, macrophages, and neutrophils²⁷. As shown in Fig. 3a, a significant decrease in the NIR fluorescence signal was observed from the scaffolds over the implantation time. Because ZW800-1 is stable in collagenase buffer (Fig. 1b) as well as in the body¹⁷, the signal reduction corresponds to the biodegraded collagen units by the enzyme (see Fig. 5b). The degree of signal reduction was notably enhanced in the axilla site compared to the thigh region. The pattern of signal reduction in both regions was similar to those from the *in vitro* test incubated with different collagenase concentrations: 0.5 mg/mL collagenase for axilla scaffold and 0.1 mg/mL collagenase for thigh scaffold (Fig. 3b).

Noninvasive magnetic resonance imaging. MRI was used to confirm the tissue infiltration process into the scaffold by measuring vascular formation over 28 days in the same animal. As shown in Fig. 4a, T1-weighted MRI without contrast agent reveals little to no evidence of vasculature within the implanted scaffold as evidenced by distinct fat and tissue separation between native and implanted region (arrowheads). By administering Magnevist, the

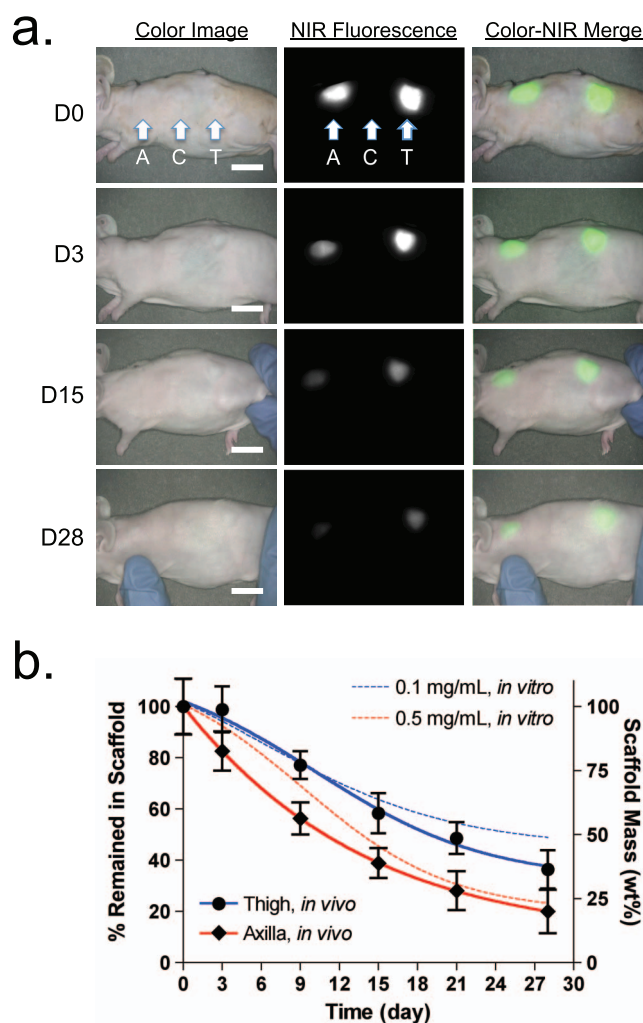


Figure 3 | Quantification of *in vivo* scaffold degradation in nude mice. (a) Optical measurements of scaffold degradation by imaging NIR fluorescence over the skin. A, axilla; C, control; T, thigh. (b) Time course of signal changes in NIR scaffolds in animals (solid lines). *In vitro* test results were added as dotted lines for comparison. ● = 0.1 mg/mL; ◆ = 0.5 mg/mL collagenase. Each data point is the mean \pm S.D. from N = 5 scaffolds. Scale bars = 1 cm.

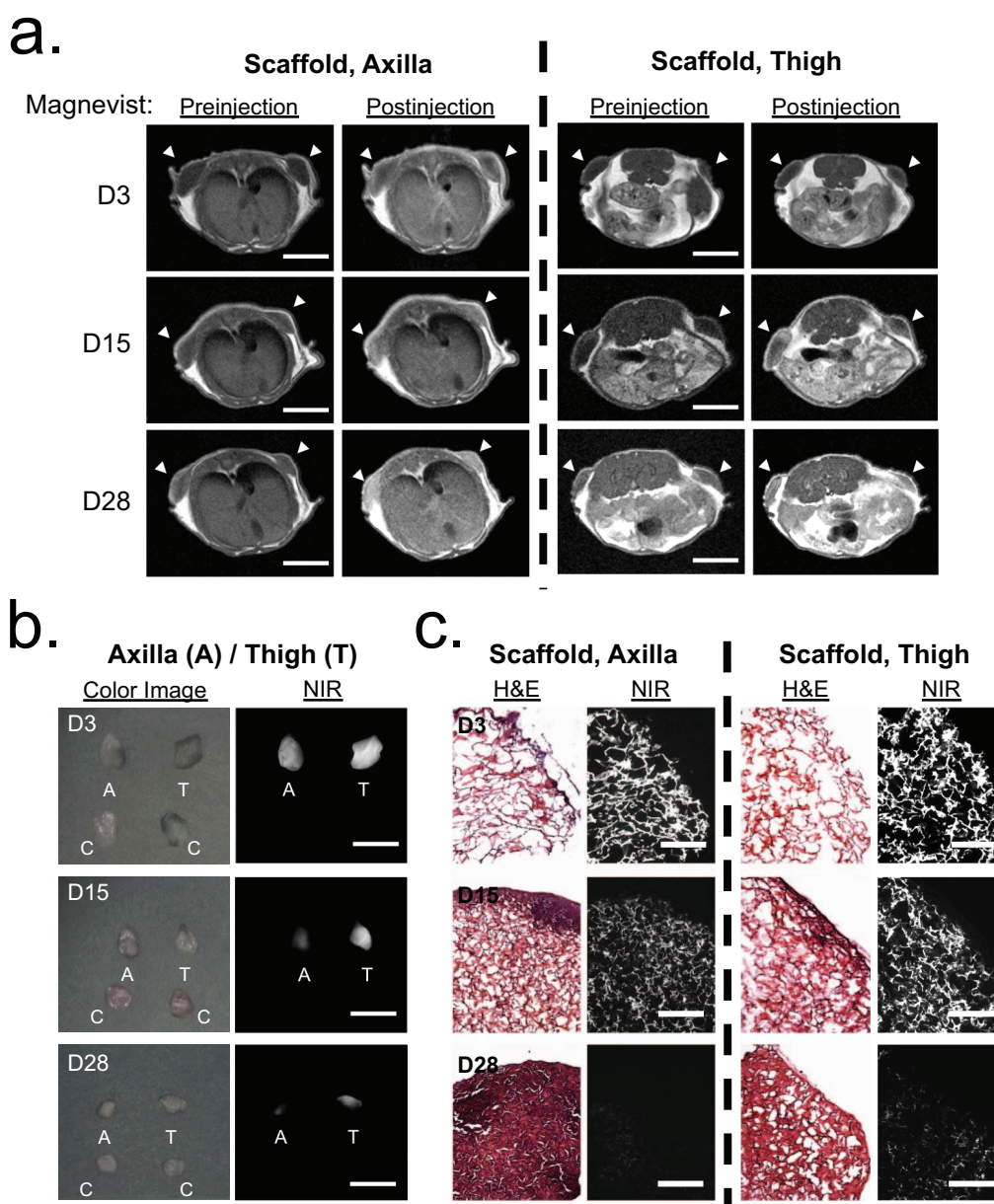


Figure 4 | Quantification of tissue ingrowth and scaffold degradation. (a) *In vivo* MR imaging of NIR scaffold implants with and without Magnevist. Arrowheads = implantation sites. (b) NIR fluorescence imaging of resected scaffolds at each time point. A, axilla; C, control; T, thigh. (c) H&E and NIR imaging of resected scaffolds from (b). Scaffold degradation accompanying tissue ingrowth was compared. Scale bars = 1 cm for (a) and (b), and 100 μ m for (c).

images show bright signal around boundaries of the implanted scaffold, which suggests onset of vascularization within and around scaffold borders. MR images of the axilla site exhibit bright and homogenous signals throughout the implanted scaffold at 28 days post-implantation due to the fully vascularized tissue. Neovascular formation in the thigh region was slower than the axillary pocket, corresponding to the slow degradation of the implanted scaffold.

Histological analysis using NIR fluorescence microscopy. In order to evaluate tissue ingrowth and inflammatory response of the tissue within the scaffold, the extracted scaffolds at each time point were observed through a NIR fluorescence microscopy after staining with hematoxylin and eosin (H&E). As shown in Fig. 4b, the size of the retrieved scaffolds was reduced over the implantation time, and the NIR fluorescence signal decreased along with the smaller scaffold. When compared to the scaffolds at the thigh region, those from the axilla were smaller in size because of faster biodegradation by

enzymes and active movement²⁸. Some inflammatory cells such as polymorphonuclear cells, monocytes, and macrophages were observed around the scaffold, and the proliferating fibroblasts in granulation tissue have been recruited and deposited into the scaffold²⁷ (Figs. 4c and S5). The host tissue infiltration into the scaffold facilitated scaffold degradation and consequentially reduced signal intensity. Tissue infiltration in the axilla scaffold was faster than those from the thigh region, which is consistent with the fluorescence and MR images.

In vivo biodistribution and clearance. To determine the bio-distribution and clearance of degraded collagen units from the NIR scaffold in the body, whole-body optical imaging was performed using the FLARETM imaging system. As shown in Fig. 5a, the biodegraded scaffold was found mainly in the kidneys and bladder. The NIR fluorescence signal decreased over the period of implantation time, and only a small amount of signal was observed

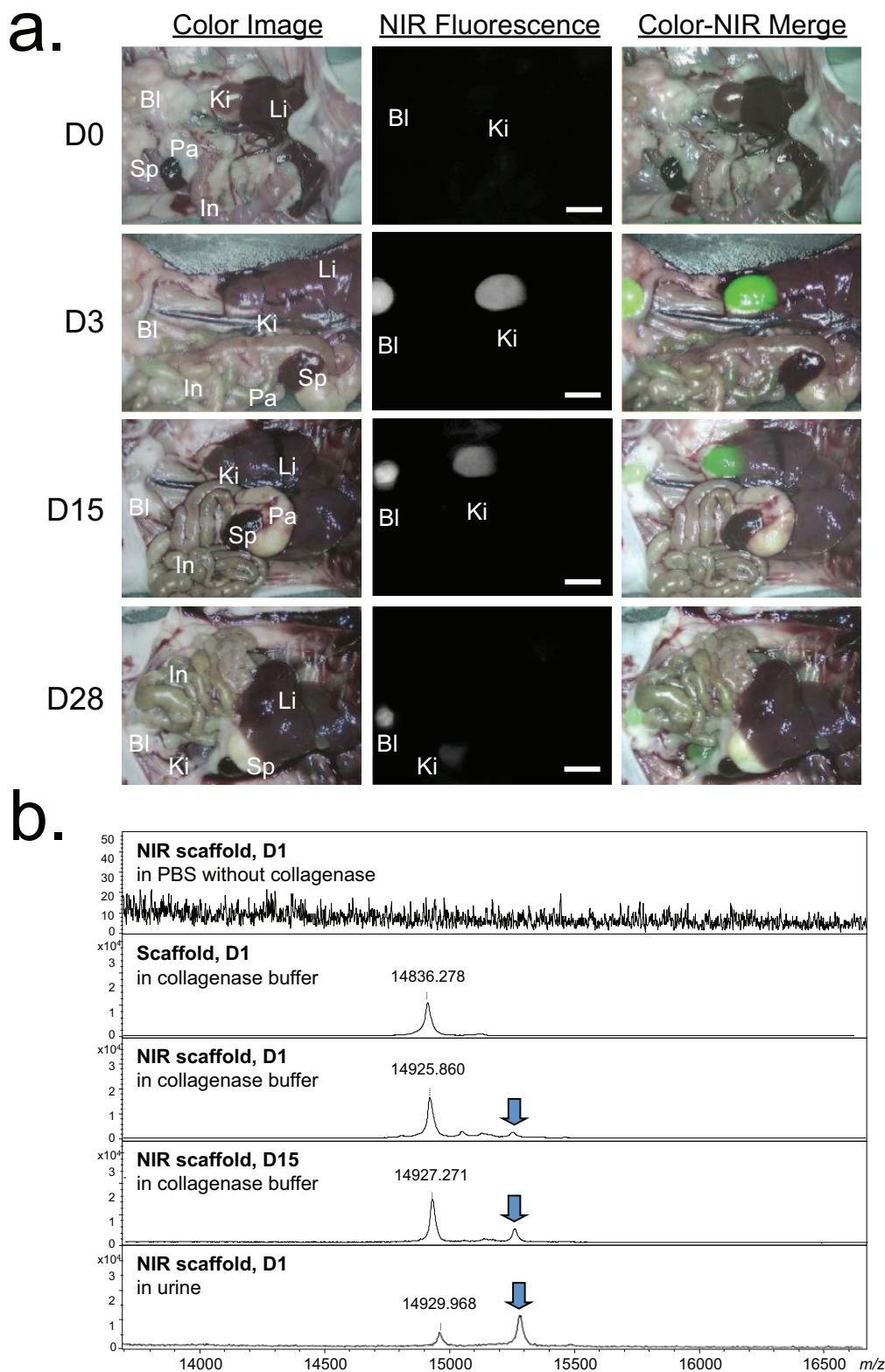


Figure 5 | Optical imaging and MALDI-TOF analysis of biodegraded scaffold over time. (a) Biodistribution and clearance of released NIR-scaffold units from the implantation site. Abbreviations used are: Bl, bladder; In, intestine; Ki, kidney; Li, liver; Pa, pancreas; Sp, spleen. Shown are color image, NIR fluorescence image, and a pseudo-color merged image of the two. Scale bars = 1 cm. (b) MALDI-TOF analysis of degraded scaffold in buffers and urine. Samples were filtered by a desalting microcolumn, packed with porous R2 resin before the measurement.

in the animal sacrificed 4 weeks post-implantation. This result demonstrates that the NIR scaffold could be removed completely from the body after it has performed its mechanical supporter function during tissue ingrowth. To investigate whether the NIR

signal is from the degraded fluorophore or from the conjugated scaffold unit, *in vitro* incubation media and *in vivo* urine samples were collected at various time points, and the molecular weight difference was measured using MALDI-TOF MS spectrometry



(Figs. 5b and S6). A control collagen scaffold without fluorophore conjugation incubated for 1 day in 0.5 mg/mL collagenase buffer showed multiple monomeric collagen-like structures around m/z of 14,930, while the fluorophore-conjugated scaffold showed higher molecular weights consistently in the *in vitro* degradation media and in the urine sample. An NIR scaffold incubated in collagenase-free buffer showed no peak in the range of 2,000 to 30,000 Da, which means no enzyme-mediated degradation happens without collagenase. To confirm whether ZW800-1 solely degraded in buffers and urine, a lower mass range (50–2,500 Da) was also scanned using MALDI-TOF (Fig. S6). Because ZW800-1 is highly stable in collagenase buffer (Fig. 1b; > 98%, 24 h), only the intact molecular mass of dye was detected by MALDI-TOF at 1 day post-incubation. On the other hand, none of the degraded ZW800-1 peak was observed from NIR scaffolds in buffers or in urine samples at the lower mass range.

Discussion

Although biodegradable scaffolds have been successfully used for tissue engineering and regenerative medicine in humans, the detailed process for scaffold degradation and tissue formation is not fully understood. Conventional techniques for measuring scaffold degradation require a large number of samples and animals to be sacrificed at every single time point, thus resulting in an inaccurate conclusion because of nonsequential measurements from different samples. Noninvasive imaging techniques such as ultrasound elasticity imaging (UEI)¹¹ and MRI¹² have been developed to monitor longitudinal tissue growth; however, these imaging modalities cannot provide direct evidence of matrix degradation.

When combined with MRI, optical fluorescence imaging using the NIR wavelength can be one of the solutions for monitoring scaffold degradation continuously along with tissue development. By tagging an invisible fluorophore covalently to the biodegradable scaffold, the degradation behavior of various biomaterials could be monitored in real time. Since light scattering and absorption in human tissue are the major obstacles in optical fluorescence imaging, NIR wavelength (700–900 nm) can efficiently minimize tissue autofluorescence, resulting in less background interference and enhanced signal-to-background ratio^{29–32}.

Another caveat in the tissue engineering and regenerative medicine field is that no optimum *in vitro* biodegradation condition has been reported yet to predict the enzyme-mediated scaffold degradation and tissue formation in the body. Although Artzi et al. reported a fluorescence imaging-based trafficking method to follow the erosion behavior of hydrogels and scaffolds in various conditions¹⁵, specific formulas were required to compensate the difference between *in vitro* and *in vivo* results. We could successfully overcome this problem by using direct comparison of NIR fluorescence imaging and quantitation of actual degradation in scaffolds and media simultaneously in various collagenase buffers. Indeed, we found that the rate of scaffold degradation and tissue ingrowth was closely related to the implantation site because of the natural variation of enzyme content and mechanical movement.

The question still remains as to whether optical fluorescence imaging can be used to track both scaffold degradation and tissue ingrowth simultaneously and quantitatively over the period of complete regeneration. Using dual-channel NIR wavelengths such as 700 nm and 800 nm, one color can be used to follow the fate of the scaffold and the other to follow the growth of tissue in the body. Although this technique has been extensively applied in image-guided surgery, current fluorescence imaging is limited by the low penetration and resolution of light up to several millimeters^{29,30}. Diffuse optical tomography and photoacoustic tomography are actively investigated in the imaging field to overcome this limitation for deep tissue imaging. Another solution is the use of multimodal imaging techniques using NIR fluorophore-tagged scaffolds and

pre-labeled stem cells or primary cells for combined MRI, CT or bioluminescence imaging to follow neo-tissue formation along with matrix degradation. In any case, NIR fluorescence imaging will play a key role in trafficking the fate of implanted materials in the body, which will initiate a new era of tissue engineering and regenerative medicine.

Methods

Engineering NIR fluorescent scaffolds. The biodegradable scaffold using porcine small intestinal submucosa (SIS) was prepared as previously reported^{20,22} (also see Supplementary Methods). An 800 nm NIR fluorescence emitting ZW800-1¹⁷ was conjugated on the scaffold using conventional *N*-hydroxysuccinimide (NHS) ester chemistry in phosphate buffer at pH 8.0. After rinsing the unconjugated dyes in distilled water 5 times, the washing solutions were collected to calculate the final labeling ratio (λ_{\max} at 770 nm, extinction coefficient = 246,000 L mol⁻¹ cm⁻¹ in PBS). As shown in Table S1, the final quantity of ZW800-1 on the scaffold was calculated by subtracting the unconjugated free dyes from the washing solutions.

In vitro scaffold degradation measurements. The NIR scaffolds (1.4 cm diameter × 0.8 cm height) were placed in 20 mL vials containing 5 mL collagenase (collagenase Type I, MP Biomedicals, LLC, OH) in PBS, pH 7.4. These vials were incubated on a shaker table set at 50 rpm and 37°C for various time periods of up to 4 weeks. At 3-day intervals, the entire media was taken for degradation analysis and replaced with 5 mL of fresh collagenase solution. For scaffold imaging, NIR scaffolds were washed 5 times in distilled water and imaged in fresh solutions using the FLARE imaging system. Solutions used for scaffold washing were added to the measurement. The NIR images were normalized and the signal intensity was quantified using ImageJ software (ver. 1.45q). The dye quantity released from the scaffold was measured using a fluorospectrometer at 770 nm excitation and 790 nm emission. The degradation pattern was plotted as accumulated-release profile over the time course of 4 weeks. At each time point, at least 5 scaffolds were collected to measure the mass loss after freeze-drying for 2 days. Mass loss was calculated using the following equation: $W_1/W_0 \times 100$ (%), where W_0 indicates the original scaffold weight and W_1 means degraded scaffold weight after lyophilization.

Animal models for scaffold implantation. Animals were housed in an AAALAC-certified facility, and all animal studies were performed under the supervision of Beth Israel Deaconess Medical Center's Institutional Animal Care and Use Committee (IACUC) in accordance with approved institutional protocol #155-2008. NCRNU nude mice (20–30 g, 6–8 weeks) were purchased from Taconic Farms (Germantown, NY). Prior to transplant scaffolds, mice were anesthetized with an intraperitoneal injection of ketamine (100 mg/kg) and xylazine (10 mg/kg). NIR scaffolds pre-wetted with Matrigel (BD Bioscience, Bedford, MA) were implanted into the subcutaneous pocket of axilla and thigh region, respectively. An unconjugated scaffold (control) was also transplanted in the middle of 2 NIR scaffold sites to retain space among scaffolds. Noninvasive optical imaging was performed from the same animal every 3 days using the FLARE imaging system. One animal at each time point was sacrificed to quantify the biodistribution of the degraded scaffolds, and the implanted constructs were harvested to use for histological analysis after H&E staining (see below).

NIR fluorescence microscopy. For microscopic imaging, scaffolds were collected and extracted from *in vitro* and *in vivo* study, fixed in 4% formalin for 10 min, molded with Tissue-Tek OCT compound (Fisher Scientific, Pittsburgh, PA), and frozen in liquid nitrogen. Frozen sections were cut to a 20 μ m thickness, and their structure and degradation pattern were examined by a 4-channel fluorescence microscope (see Supplementary Methods).

Optical imaging system and quantification. The real-time intraoperative FLARETM imaging system has been described in detail previously^{33,34}. In this study, a custom filter set (Chroma Technology Corporation, Brattleboro, VT) composed of a 750 \pm 25 nm excitation filter, a 785 nm dichroic mirror, and an 810 \pm 20 nm emission filter, with white light (400 to 650 nm) at 40,000 lx were used to detect NIR fluorescence signals. Color and NIR fluorescence images were acquired simultaneously with custom software at rates up to 15 Hz over a 15 cm diameter field of view. A pseudo-colored green was used for NIR fluorescence in the color-NIR merged images. At each time point, the fluorescence (FL) and background (BG) intensity of a region of interest (ROI) over each organ/tissue was quantified using ImageJ software. The contrast-to-background ratio (CBR) was calculated as $CBR = FL/BG - 1$. To quantify dye contents in the scaffold and from the released solution, NIR scaffolds in collagenase-free buffers were used as a control, and the signal changes were applied to the final quantification. For scaffold-implanted animals, the CBR was measured using an ROI over the scaffold for FL and an ROI over the skin for BG³⁵. At least 5 animals were analyzed at each time point. Statistical analysis was carried out using a one-way ANOVA followed by Tukey's multiple comparisons test. Results were presented as mean \pm S.D. and curve fitting was performed using Prism version 4.0a software (GraphPad, San Diego, CA).

Magnetic resonance imaging (MRI). To confirm tissue formation in the scaffold, 1T micro MRI system (Aspect, Israel) was used. 50 μ L of Magnevist (Berlex Imaging,



Wayne, NJ) diluted 10-fold in saline was injected in the tail vein to track tissue formation by vascularization. The imaging protocol consisted of T1-weighted spin echo sequence with TR/TE = 412.6/10.9 ms, matrix size = 256 × 256, slice thickness = 2.0 mm, gap = 0.0 mm, field of view = 60 mm.

- Langer, R. & Vacanti, J. P. Tissue engineering. *Science* **260**, 920–926 (1993).
- Atala, A. Tissue engineering and regenerative medicine: concepts for clinical application. *Rejuvenation Res* **7**, 15–31 (2004).
- Lee, S. J., Van Dyke, M., Atala, A. & Yoo, J. J. Host cell mobilization for in situ tissue regeneration. *Rejuvenation Res* **11**, 747–756 (2008).
- Hutmacher, D. W. Scaffolds in tissue engineering bone and cartilage. *Biomaterials* **21**, 2529–2543 (2000).
- Middleton, J. C. & Tipton, A. J. Synthetic biodegradable polymers as orthopedic devices. *Biomaterials* **21**, 2335–2346 (2000).
- Oh, S. H. *et al.* Degradation behavior of 3D porous polydioxanone-b-polycaprolactone scaffolds fabricated using the melt-molding particulate-leaching method. *J Biomater Sci Polym Ed* **22**, 225–237 (2011).
- Lee, S. J. *et al.* Development of a composite vascular scaffolding system that withstands physiological vascular conditions. *Biomaterials* **29**, 2891–2898 (2008).
- Cho, H. & An, J. The effect of epsilon-caproyl/D,L-lactyl unit composition on the hydrolytic degradation of poly(D,L-lactide-ran-epsilon-caprolactone)-poly(ethylene glycol)-poly(D,L-lactide-ran-epsilon-caprolactone). *Biomaterials* **27**, 544–552 (2006).
- Agrawal, C. M., McKinney, J. S., Lanctot, D. & Athanasiou, K. A. Effects of fluid flow on the in vitro degradation kinetics of biodegradable scaffolds for tissue engineering. *Biomaterials* **21**, 2443–2452 (2000).
- Agnihotri, S. A., Kulkarni, V. D., Kulkarni, A. R. & Aminabhavi, T. M. Degradation of chitosan and chemically modified chitosan by viscosity measurements. *J Appl Polym Sci* **102**, 3255–3258 (2006).
- Kim, K., Jeong, C. G. & Hollister, S. J. Non-invasive monitoring of tissue scaffold degradation using ultrasound elasticity imaging. *Acta Biomater* **4**, 783–790 (2008).
- Saldanha, K. J., Piper, S. L., Ainslie, K. M., Kim, H. T. & Majumdar, S. Magnetic resonance imaging of iron oxide labelled stem cells: applications to tissue engineering based regeneration of the intervertebral disc. *Eur Cell Mater* **16**, 17–25 (2008).
- Yang, Y., Yiu, H. H. & El Haj, A. J. On-line fluorescent monitoring of the degradation of polymeric scaffolds for tissue engineering. *Analyst* **130**, 1502–1506 (2005).
- Murphy, C. L. & Lever, M. J. A ratiometric method of autofluorescence correction used for the quantification of Evans blue dye fluorescence in rabbit arterial tissues. *Exp Physiol* **87**, 163–170 (2002).
- Artzi, N. *et al.* In vivo and in vitro tracking of erosion in biodegradable materials using non-invasive fluorescence imaging. *Nat Mater* **10**, 704–709 (2011).
- Nakayama, A., del Monte, F., Hajjar, R. J. & Frangioni, J. V. Functional near-infrared fluorescence imaging for cardiac surgery and targeted gene therapy. *Mol Imaging* **1**, 365–377 (2002).
- Choi, H. S. *et al.* Synthesis and in vivo fate of zwitterionic near-infrared fluorophores. *Angew Chem Int Ed Engl* **50**, 6258–6263 (2011).
- Tanaka, E., Choi, H. S., Fujii, H., Bawendi, M. G. & Frangioni, J. V. Image-guided oncologic surgery using invisible light: completed pre-clinical development for sentinel lymph node mapping. *Ann Surg Oncol* **13**, 1671–1681 (2006).
- Choi, H. S. *et al.* Targeted zwitterionic near-infrared fluorophores for improved optical imaging. *Nat Biotechnol*, in press (2013).
- Badylak, S. F., Record, R., Lindberg, K., Hodde, J. & Park, K. Small intestinal submucosa: a substrate for in vitro cell growth. *J Biomater Sci Polym Ed* **9**, 863–878 (1998).
- Lindberg, K. & Badylak, S. F. Porcine small intestinal submucosa (SIS): a bioscaffold supporting in vitro primary human epidermal cell differentiation and synthesis of basement membrane proteins. *Burns* **27**, 254–266 (2001).
- Kim, M. S. *et al.* Preparation of sponge using porcine small intestinal submucosa and their applications as a scaffold and a wound dressing. *Adv Exp Med Biol* **585**, 209–222 (2006).
- Lee, S. J., Lee, I. W., Lee, Y. M., Lee, H. B. & Khang, G. Macroporous biodegradable natural/synthetic hybrid scaffolds as small intestine submucosa impregnated poly(D,L-lactide-co-glycolide) for tissue-engineered bone. *J Biomater Sci Polym Ed* **15**, 1003–1017 (2004).
- Hyun, H. *et al.* cGMP-Compatible preparative scale synthesis of near-infrared fluorophores. *Contrast Media Mol Imaging* **7**, 516–524 (2012).
- Gopferich, A. Mechanisms of polymer degradation and erosion. *Biomaterials* **17**, 103–114 (1996).
- Hilborn, J. & Bjursten, L. M. A new and evolving paradigm for biocompatibility. *J Tissue Eng Regen Med* **1**, 110–119 (2007).
- Gross, J. *et al.* Animal collagenases: specificity of action, and structures of the substrate cleavage site. *Biochem Biophys Res Commun* **61**, 605–612 (1974).
- Friess, W. Collagen-biomaterial for drug delivery. *Eur J Pharm Biopharm* **45**, 113–136 (1998).
- Frangioni, J. V. In vivo near-infrared fluorescence imaging. *Curr Opin Chem Biol* **7**, 626–634 (2003).
- Gioux, S., Choi, H. S. & Frangioni, J. V. Image-guided surgery using invisible near-infrared light: fundamentals of clinical translation. *Mol Imaging* **9**, 237–255 (2010).
- Lee, J. H., Park, G., Hong, G. H., Choi, J. & Choi, H. S. Design considerations for targeted optical contrast agents. *Quant Imaging Med Surg* **2**, 266–273 (2012).
- Gibbs, S. L. Near infrared fluorescence for image-guided surgery. *Quant Imaging Med Surg* **2**, 177–187 (2012).
- Choi, H. S. *et al.* Tissue- and organ-selective biodistribution of NIR fluorescent quantum dots. *Nano Lett* **9**, 2354–2359 (2009).
- Yuan, T. L. *et al.* Class 1A PI3K regulates vessel integrity during development and tumorigenesis. *Proc Natl Acad Sci USA* **105**, 9739–9744 (2008).
- Choi, H. S. *et al.* Design considerations for tumour-targeted nanoparticles. *Nat Nanotechnol* **5**, 42–47 (2010).

Acknowledgments

We thank Dr. John V. Frangioni for many helpful discussions, and Dr. Sylvain Gioux, Rafiou Oketokoun, and Alan Stockdale for assistance with development of the FLARE imaging system and software. We also thank David Burrington, Jr. for editing, and Eugenia Trabucchi for administrative assistance. This study was supported by the National Institutes of Health: NHLBI grant #HL098912 (SJL), NIBIB grant #R01-EB-010022 (HSC), and #R01-EB-011523 (HSC), and the Dana Foundation Program in Brain and Immuno-Imaging (HSC). GK and SHK were supported by WCU Program (R31-20029) from the Korea Ministry of Education, Science and Technology (KMEST).

Author contributions

S.H.K., J.H.L., H.H., Y.A., E.L., and K.R. performed the experiments. S.H.K., S.J.L., G.P., G.K., and H.S.C. reviewed, analyzed, and interpreted the data. S.H.K., S.J.L., G.P., G.K., and H.S.C. wrote the paper. All authors discussed the results and commented on the manuscript.

Additional information

Supplementary information accompanies this paper at <http://www.nature.com/scientificreports>

Competing financial interests: The authors declare no competing financial interests.

License: This work is licensed under a Creative Commons Attribution-NonCommercial-NoDerivs 3.0 Unported License. To view a copy of this license, visit <http://creativecommons.org/licenses/by-nc-nd/3.0/>

How to cite this article: Kim, S.H. *et al.* Near-Infrared Fluorescence Imaging for Noninvasive Trafficking of Scaffold Degradation. *Sci. Rep.* **3**, 1198; DOI:10.1038/srep01198 (2013).